PCCP

PAPER

View Article Online
View Journal | View Issue



Cite this: *Phys. Chem. Chem. Phys.*, 2015, **17**, 8750

# Anion and cation dynamics of sulfonylamide-based ionic liquids and the solid–liquid transitions

Mamoru Imanari,[a] Kozo Fujii,[b] Tomohiro Mukai,[c] Noriko Mizushima,[d] Hiroko Seki[a] and Keiko Nishikawa*[b]

Received 17th January 2015,
Accepted 20th February 2015

DOI: 10.1039/c5cp00302d

www.rsc.org/pccp

Some of the important factors that characterise room-temperature ionic liquids (RTILs) are the variety of conformations adopted by the constituent ions and their flexibility. Using 1,3-dimethylimidazolium bis(fluorosulfonyl)amide ([$C_1$mim][FSA]) and 1,3-dimethylimidazolium bis(trifluoromethylsulfonyl)amide ([$C_1$mim][$NTf_2$]) as samples, the longitudinal and transverse relaxation times ($T_1$ and $T_2$) for $^{19}$F and $^{1}$H were determined as a function of temperature and were correlated with the dynamics of the phase behaviours of the two RTILs. Because the anions and cations in the two compounds have $^{19}$F and $^{1}$H nuclei, respectively, their dynamics can be independently investigated and the relationships between them can be discussed. For [$C_1$mim][FSA], the only observed phase changes included melting and crystallisation. The temperature dependences of $T_1$ and $T_2$ for $^{19}$F were similar to those of $T_1$ and $T_2$ for $^{1}$H, indicating similar dynamics due to the formation of strong anion–cation interactions. For [$C_1$mim][$NTf_2$], the $T_1$ and $T_2$ values for both $^{19}$F and $^{1}$H discontinuously changed at same temperatures, which were assigned to the crystallisation and melting points. However, the $T_1$ curves for $^{19}$F and $^{1}$H were different in the crystalline region, suggesting independent dynamics for the anions and cations in [$C_1$mim][$NTf_2$]. In the crystalline state for each salt, the cation dynamics was distinctly separated into the framework movement of the imidazolium ring and the movement of the methyl groups, while the anion dynamics was characterised by the movement of the entire anion. The influence of the crystal structure on the dynamics of each salt was also considered.



## 1. Introduction

Room-temperature ionic liquids (RTILs) constitute a new class of liquids that have attracted much attention due to their characteristic properties[1–5] and potential application as functional liquids.[5–15] Unique properties are remarkably manifested in the thermal behaviours of RTILs, such as low melting points despite being composed only of ions, hardness upon crystallisation, pre-melting over a wide temperature range, excessive supercooling and complex thermal histories.[16–27] Extremely slow dynamics during phase changes is another characteristic phenomenon in many ionic liquids.[23–25,28,29] These phenomena are proved to be closely related to the variety and flexibility of the conformations of the constituent ions.[1,30,31] Many research groups have focused on cations of imidazolium-based RTILs and investigated phase behaviours linked to conformational changes of the substituent groups of each cation, by calorimetry,[22–27] Raman spectroscopy[1,26,27,32–35] and nuclear magnetic resonance (NMR) analyses.[29,36–48] Previously, we revealed a relationship between the thermodynamic properties of imidazolium-based RTILs and their cation dynamics.[22–27,29,44–48] However, studies on the flexibility of RTIL ions are mainly limited to cations.

In the present study, attention was thus focused on the anion dynamics of sulfonylamide-based RTILs to reveal the phase behaviours linked to those dynamics. The longitudinal and transverse relaxation times ($T_1$ and $T_2$, respectively) for $^{19}$F as a function of temperature were determined over a wide temperature range for RTILs with the two amide anions, bis(fluorosulfonyl)amide ($[FSA]^-$) and bis(trifluoromethylsulfonyl)amide ($[NTf_2]^-$) (see Fig. 1 for the chemical structures). $[FSA]^-$ and $[NTf_2]^-$ are the most well-known anions for RTILs. The cation 1,3-dimethylimidazolium ($[C_1mim]^+$) was used in both RTILs because it has no conformational flexibility other than the rotation of methyl groups around the N–C axes. Consequently, the flexibilities of the anion groups and the dynamics triggered by their flexible motions could be more easily investigated. In addition, the $T_1$ and $T_2$ values for $^{1}$H were measured. Specifically, because the anions and cations in the

[a] *Center for Analytical Instrumentation, Chiba University, Yayoi-cho, Inage-ku, Chiba 263-8522, Japan*
[b] *Graduate School of Advanced Integration Science, Chiba University, Yayoi-cho, Inage-ku, Chiba 263-8522, Japan. E-mail: k.nishikawa@faculty.chiba-u.jp*
[c] *Science Research Center, Hosei University, Fujimi, Chiyoda-ku, Tokyo 102-8160, Japan*
[d] *Laboratory of Clinical Pharmacy, Yokohama College of Pharmacy, Matano-cho, Totsuka-ku, Yokohama 245-0066, Japan*

 

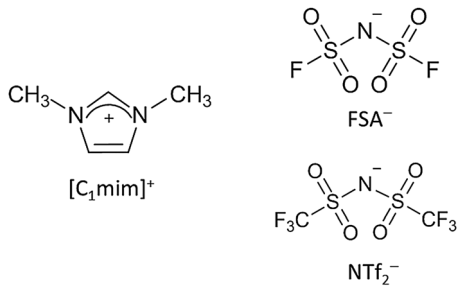


Fig. 1 Chemical structures of the cation ($[C_1mim]^+$) and anions ($[FSA]^-$ and $[NTf_2]^-$).

two RTILs have $^{19}F$ and $^{1}H$ nuclei, respectively, the dynamics of the anions and cations could be independently revealed and then the relationships between them can be evaluated.

Furthermore, these sulfonylamide anions are suggested to be highly non-coordinatable ions due to their broadly delocalised negative charges and large internal flexibility.[49–52] Accordingly, by determining the $^{1}H$ and $^{19}F$ relaxation times, identification of the phase behaviours linked to differences in the anions should be possible.

## 2. Experimental

The samples, $[C_1mim][FSA]$ and $[C_1mim][NTf_2]$, were synthesised following a previously established procedure[53] as described in the supporting information of our recent paper.[54] The purity of each sample was confirmed by $^{1}H$ and $^{13}C$ NMR and elemental analyses. No impurity signals were observed in the NMR spectra.

To determine the general thermal phase behaviours of the samples, calorimetric measurements of sufficiently dried samples (1–2 mg) were performed using a laboratory-made calorimeter with a baseline stability of $\pm 5$ μW and a thermal stability of 0.001 K.[34] Measurements for both samples were performed at a scanning rate of 5 mK $s^{-1}$ for the cooling and heating processes.

Samples for the NMR analyses were prepared by placing each neat RTIL (approximately 0.5–1 g) into a 10 mm-diameter glass sample tube. The sample was dried for 5 h at temperatures above 373 K under a $10^{-3}$ Pa vacuum to remove water and volatile contaminants that could affect the properties of the RTIL. After drying, each sample tube was flame-sealed under the connecting vacuum line.

The $T_1$ and $T_2$ measurements for $^{19}F$ and $^{1}H$ were performed using a JEOL MU-25 pulse NMR spectrometer with a $^{19}F$ resonance frequency of 23.5 MHz and a $^{1}H$ resonance frequency of 25 MHz. At these low resonance frequencies, the overall dynamics of the anions and cations were observed because the separations of the signals according to the chemical shifts for each ion were small. The $T_1$ measurements were performed using the inversion recovery pulse sequence[55] and the saturation recovery method[56] for the states with long $T_1$ values. The $T_2$ measurements were performed using the Carr–Purcell–Meiboom–Gill (CPMG) pulse sequence for the liquid state[57,58] and the solid echo sequence for the solid state.[59,60] The temperature ranges for both samples were very wide. Each sample was first heated to a temperature of 30–40 K higher than its melting point, then cooled down to a temperature of 100–120 K lower than the melting point and subsequently warmed to the starting temperature. Measurements were performed every 10 K during which the sample was maintained at that temperature.

## 3. Results and discussion

### 3.1. Theoretical background

The homonuclear relaxation rates ($1/T_1$ and $1/T_2$) are described using the following equations for the dipolar relaxation mechanism:[61,62]

$$\frac{1}{T_1} = \frac{2\gamma^4\hbar^2 I(I+1)}{5r^6}\left[\frac{\tau_c}{1+\omega^2{\tau_c}^2} + \frac{4\tau_c}{1+4\omega^2{\tau_c}^2}\right] \quad (1)$$

and

$$\frac{1}{T_2} = \frac{\gamma^2\hbar^2 I(I+1)}{5r^6}\left[3\tau_c + \frac{5\tau_c}{1+\omega^2{\tau_c}^2} + \frac{2\tau_c}{1+4\omega^2{\tau_c}^2}\right], \quad (2)$$

where $\omega$ is the $^{19}F$ or $^{1}H$ Larmor frequency, $\gamma$ is the gyromagnetic ratio, $\hbar$ is $h/2\pi$ with $h$ representing Planck's constant, $I$ is the spin quantum number, $r$ is the inter-fluorine (or -proton) distance and $\tau_c$ is the correlation time. Eqn (1) and (2) can be applied for both $^{19}F$ and $^{1}H$. The relaxation rate $1/T_1$ is proportional to $\tau_c$ in the region where $\omega\tau_c \ll 1$ (extreme narrowing conditions) and is proportional to $1/\tau_c$ in the region where $\omega\tau_c \gg 1$. Consequently, the curve for $T_1$ *vs.* temperature in a phase has a positive slope in the higher temperature region and a negative slope in the lower temperature region, with the minimum value at $\omega\tau_c = 0.62$. On the other hand, because the relaxation rate $1/T_2$ is mainly proportional to $\tau_c$ in eqn (2), the $T_2$ values simply decrease with a decrease in temperature. If a phase change occurs, the $T_1$ and $T_2$ values should change discontinuously at that temperature. Furthermore, the temperature-dependent correlation time $\tau_c$ obeys the Arrhenius equation,[55]

$$\tau_c = \tau_A \exp\left[\frac{E_a}{RT}\right], \quad (3)$$

where $E_a$ is the activation energy, $R$ is the gas constant and $T$ is the absolute temperature. Therefore, the activation energy of reorientational motion can be estimated from the temperature dependence of the correlation time $\tau_c$.

### 3.2. $[C_1mim][FSA]$

Calorimetric measurements for $[C_1mim][FSA]$ were performed using a laboratory-made apparatus.[34] Crystalline $[C_1mim][FSA]$ was first melted completely by heating, then cooled from 370 to 210 K and subsequently heated to 370 K. The cooling and heating rates were both 5 mK $s^{-1}$. The results are presented in Fig. 2. The exothermic signal that appeared at approximately 303 K during cooling was assigned to the crystallisation process, while the endothermic signal observed at approximately 332 K during heating was attributed to the melting process.

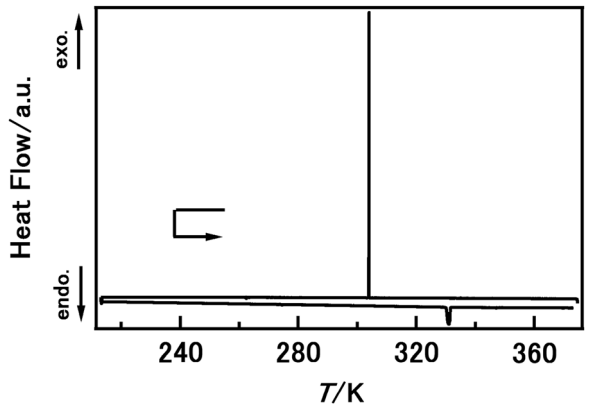


Fig. 2 Calorimetric curve for [$C_1$mim][FSA] obtained using a laboratory-made calorimeter. The scanning rate for cooling and heating was 5 mK $s^{-1}$. The crystalline sample was first melted completely by heating, then cooled from 370 to 210 K and finally heated to 370 K. The sharp exothermic signal, at approximately 303 K during the cooling process, was assigned to crystallisation; the endothermic signal, at approximately 332 K during the heating process, was attributed to melting.

Notably for this sample, crystallisation occurred sharply during cooling and melting occurred over a relatively narrow temperature range than that typically seen for imidazolium-based ionic liquids with longer alkyl chains.[22–27] In addition, no complex thermal histories were detected at the scanning rate used.

The NMR analyses for determining the $^{19}$F $T_1$ and $T_2$ values for [$C_1$mim][FSA] were performed over the temperature range from 233 to 413 K, varying the temperature by cooling from 413 to 233 K and then heating back to 413 K. At every 10 K, the measurements were performed keeping the temperature constant for each analysis. Fig. 3 shows the obtained $^{19}$F $T_1$ and $T_2$ values as a function of temperature. Both the $^{19}$F $T_1$ and $T_2$ cooling curves (black curves) discontinuously changed at 303 K, which is the temperature assigned to the crystallisation process according to the calorimetric measurements (see Fig. 2). After crystallisation, the $T_1$ values decreased as the temperature decreased, reaching a minimum at approximately 283 K. The correlation time for $^{19}$F reorientational dynamics at 283 K was calculated to be approximately 4.2 ns using the relationship $\omega\tau_c = 0.62$ at the minimum point. After passing through the minimum point, the $T_1$ values then increased exponentially as the temperature decreased. On the other hand, the $T_2$ values remained nearly constant at 40 μs after crystallisation. During heating (red symbols), the $^{19}$F $T_1$ and $T_2$ values followed the corresponding $T_1$ and $T_2$ traces for the cooling process except in the super-cooled region from 303 to 333 K and discontinuously changed at approximately 333 K. This temperature corresponds to the melting temperature observed in the calorimetric measurements (see Fig. 2). After melting, both the $^{19}$F $T_1$ and $T_2$ values perfectly followed the corresponding $T_1$ and $T_2$ traces obtained during cooling.

The $^1$H $T_1$ and $T_2$ values for [$C_1$mim][FSA] as a function of temperature are shown in Fig. 4. Like the temperature dependence curves of the $^{19}$F $T_1$ and $T_2$ values, the $^1$H $T_1$ and $T_2$ curves changed discontinuously at approximately 303 K during cooling and 333 K during heating, the temperatures are assigned to the crystallisation and melting processes, respectively. In addition, in the crystalline state, the value of $^1$H $T_1$ reached a minimum at the same temperature as that for $^{19}$F $T_1$, and the $^1$H $T_2$ values remained constant at 22 μs. The temperature dependence curves of the $^1$H $T_1$ and $T_2$ values during heating (red symbols) also behaved similarly to those obtained during cooling (black symbols), except in the super-cooled region. The activation energy estimated from the linear part of the $^1$H $T_1$ trace during heating was 12.9 kJ $mol^{-1}$. This value corresponds well to the rotational energy of the C–$CH_3$ axis in [$C_4$mim]Cl determined using inelastic neutron scattering experiments.[63] Therefore, it is possible to conclude that the correlation time

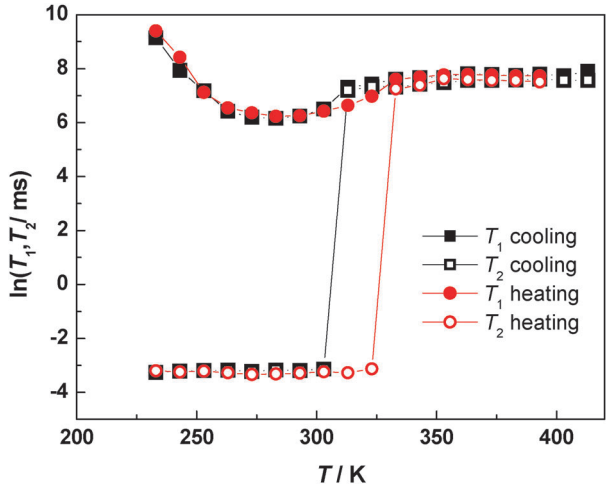


Fig. 3 $^{19}$F $T_1$ and $T_2$ values for [$C_1$mim][FSA] as a function of temperature obtained using a $^{19}$F pulse NMR spectrometer. The temperature was varied according to the following cycle: cooling from 413 to 233 K followed by heating to 413 K. Measurements were obtained every 10 K, keeping the temperature constant. The discontinuous points in the $T_2$ curve near 303 K during cooling and 333 K during heating correspond to the crystallisation and melting points, respectively.

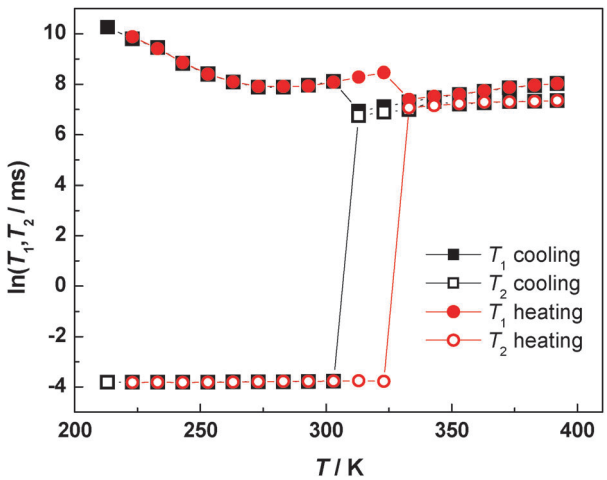


Fig. 4 $^1$H $T_1$ and $T_2$ values for [$C_1$mim][FSA] as a function of temperature obtained using a $^1$H pulse NMR spectrometer. The temperature was varied in the same manner as described in Fig. 3.

 

$\tau_c$ = 3.95 ns derived from the $T_1$ minimum point at approximately 283 K is associated with the rotational motion of methyl groups in the crystalline phase.

Comparing the cooling curves for $^{19}$F $T_1$ (black closed squares in Fig. 3) and $^1$H $T_1$ (black closed squares in Fig. 4), it can be seen that the values for $^1$H in the liquid state jumped to higher values during the phase change to the crystalline state at 303 K, while those for $^{19}$F jumped to lower values. Moreover, the discontinuity for $^1$H $T_1$ at the phase change was more remarkable than that for $^{19}$F $T_1$. These results are interpreted as follows. If neglecting the interactions between ions is possible, then the observed correlation time ($\tau_{obs}$) can be separated into two contributions:

$$1/\tau_{obs} = 1/\tau_{frame} + 1/\tau_{local}, \quad (4)$$

where $\tau_{frame}$ and $\tau_{local}$ are the correlation times from the frame of the ion and the internal local motion in the ion, respectively. In the [$C_1$mim] cation, $\tau_{frame}$ corresponds to the correlation time for the imidazolium ring, and this value became very large at the crystallisation point. Therefore, the longitudinal relaxation time $T_{1,frame}$ due to the dipole–dipole interaction, which is given by eqn (1), became very large. Consequently, in the observed values ($T_{1,obs}$) is calculated by the following relationship:

$$1/T_{1,obs} = 1/T_{1,frame} + 1/T_{1,local}, \quad (5)$$

$1/T_{1,frame}$ can be neglected. Parameter $T_{1,local}$ corresponds to the contribution from the rotation of the methyl groups. Fig. 4 shows that only the contribution from the methyl groups appears in the $T_1$ curve in the crystalline state and the methyl groups in the cation move actively even after crystallisation, while the frame of the cation, namely the imidazolium ring, is frozen. The activation energy of the rotation of the methyl groups was 12.9 kJ mol$^{-1}$, as described above. For the [FSA] anion, on the other hand, distinctly separating the frame and local parts according to their movements was impossible.

Aside from the above-mentioned trend, the behaviours of the temperature-dependent $^1$H $T_1$ and $T_2$ curves, namely the crystallisation and melting points and minimum $T_1$ values, were in perfect agreement with those observed for the $^{19}$F $T_1$ and $T_2$ curves. The correlation time for $^{19}$F at 283 K was approximately 4.2 ns, which is very close to the $^1$H correlation time of 3.95 ns. These results suggested the same dynamics of the anion and the cation due to the formation of strong interactions.

Recently we reported the crystal structure of [$C_1$mim][FSA] determined *via* single-crystal X-ray diffraction.[54] Therefore, the dynamics of the salt in the crystalline state was considered in relation to the crystal structure. First, the magnitudes of the $^{19}$F $T_1$ values were compared before and after crystallisation. The $^{19}$F $T_1$ values were nearly the same for the liquid and crystalline states, although $^{19}$F $T_2$ clearly showed a discontinuous change. In the crystalline state, the conformation of the [FSA]$^-$ ion is a perfectly symmetric cisoid,[54] while transoid conformers are partially included in the liquid state as described later. As a result, the average internal distance between F atoms for the liquid state is longer than the one for the crystalline state. Because the value of $T_1$ is proportional to the sixth power of the distance between dipoles as shown in eqn (1), the $^{19}$F $T_1$ values for the liquid state are larger. This is the reason why the jump of $^{19}$F $T_1$ values during crystallisation became smaller.

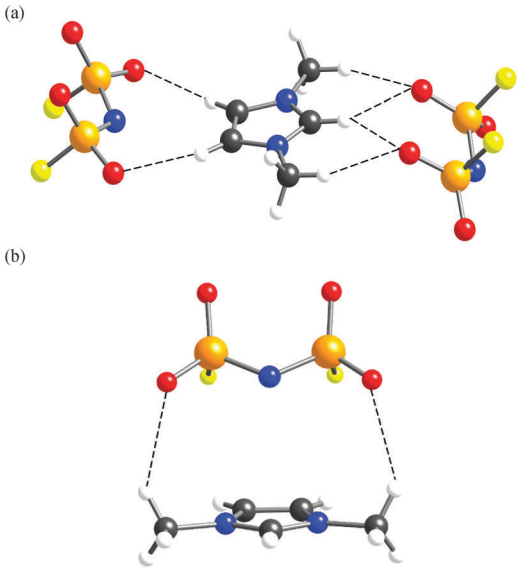


Fig. 5 (a) In-plane hydrogen bonding and (b) out-of-plane hydrogen bonding in a [$C_1$mim][FSA] crystal. Grey: carbon, blue: nitrogen, yellow: fluorine, orange: sulfur, red: oxygen and white: hydrogen.

Second, the contribution of hydrogen bonding was evaluated. As can be seen in Fig. 5(a) and (b), the structure of the crystal is characterised by three types of hydrogen bonds.[54] The strongest hydrogen bond in the crystal is formed between two O atoms in an anion and three H atoms in a cation to generate a characteristic W-shaped tridentate bonding arrangement (see Fig. 5(a)). The second strongest hydrogen bond is formed between two O atoms in an anion and two of the H atoms attached to an imidazolium ring of a cation. As shown in Fig. 5(b), two O atoms in an anion also form weaker hydrogen bonds with two H atoms in the methyl groups of a cation to form the third and weakest type of hydrogen bond. Surprisingly, no F atoms take part in hydrogen bonding. N($SO_2$R)$_2$-type anions are well known to be characterised by the large flexibility of the $SO_2$ groups around the S–N axes.[52,64,65] However, for [$C_1$mim][FSA], the movement of the $SO_2$ groups in the anion is hindered by the strong hydrogen bonds with the cation. The motion of the F atoms is also restricted, because each F atom is directly bonded to each S atom. The motion of the methyl groups in the cation is also hindered. Furthermore, all three types of hydrogen bonding can occur between a single anion and a single cation, as shown in Fig. 5(a) and (b). In such a way, the anion and the cation are connected with very rigid and strong interactions, which were reflected in a similar reorientational dynamics observed for the cation and the anion of [$C_1$mim][FSA] in the crystalline state. Even in the liquid state, we can assume that the anion and the cation form strong pairs, which is possible due to the strong hydrogen bonding that occurs between them in addition to Coulomb interactions.

Looking again at Fig. 3 and 4, it can be seen that after passing through the minimum point, both the $^{19}$F and $^{1}$H $T_1$ values increased exponentially, as the temperature decreased, to large values of 15 and 20 s, respectively, at 223 K. These values are extremely large compared to those for crystalline [$C_1$mim][$NTf_2$] as described later and [$C_n$mim]Br[29,43,44] and suggest that [$C_1$mim][FSA] forms a hard crystal due to the ordering of the constituent ions with high symmetries and the strong hydrogen bonding[54] described above.

Using Raman spectroscopy, two stable conformers of the $[FSA]^-$ ion, cisoid and transoid, were confirmed to coexist in the liquid state of [$C_1$mim][FSA], as in the case of [$C_2$mim][FSA].[52] On the other hand, in the crystalline state, [$C_1$mim][FSA] only adopts the cisoid conformation.[54] Therefore, the phase transition (melting during heating) and structural relaxation (crystallisation during cooling) of [$C_1$mim][FSA] can be found to occur due to the cisoid–transoid conformational change of a portion of $[FSA]^-$ ions.

### 3.3. [$C_1$mim][$NTf_2$]

The calorimetric data for [$C_1$mim][$NTf_2$] are presented in Fig. 6. The exothermic signal at 283 K during cooling and the endothermic signal at 298 K during heating were assigned to the crystallisation and melting points, respectively. Like for [$C_1$mim][FSA], crystallisation of [$C_1$mim][$NTf_2$] occurred sharply during cooling, and no complex thermal histories were detected at a scanning speed of 5 mK $s^{-1}$. Although a pre-melting phenomenon was observed, the temperature range was relatively narrow compared to those of imidazolium-based ionic liquids with longer alkyl chains, such as $[C_4mim]^+$ salts.[22–27] In addition, the temperature range of the super-cooled region was 15 K under the experimental conditions used in the present study and was relatively narrow than those of imidazolium-based RTILs with the cation flexibility.

The $^{19}$F $T_1$ and $T_2$ values plotted as a function of temperature in Fig. 7 revealed the dynamics of the anion in [$C_1$mim][$NTf_2$]. They both discontinuously changed at approximately 283 K

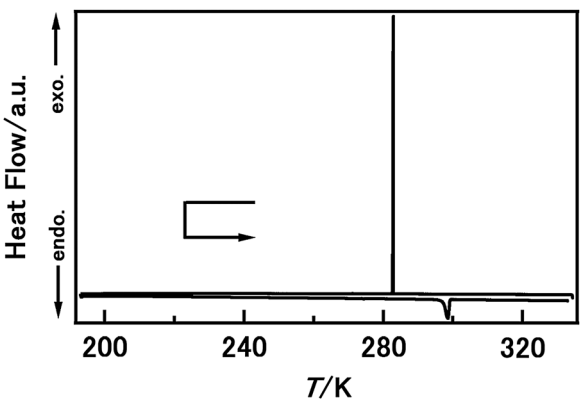


Fig. 6 Calorimetric curve for [$C_1$mim][$NTf_2$] obtained using a laboratory-made calorimeter. The scanning rate for cooling and heating was 5 mK $s^{-1}$. The sharp exothermic signal at 283 K during cooling and the endothermic signal at 298 K during heating were assigned to crystallisation and melting, respectively.

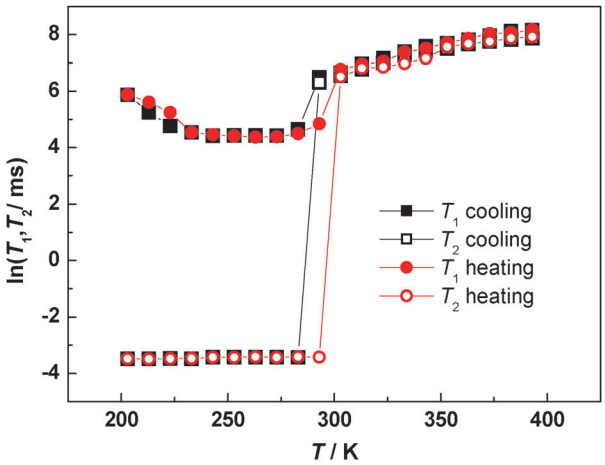


Fig. 7 $^{19}$F $T_1$ and $T_2$ values for [$C_1$mim][$NTf_2$] as a function of temperature obtained using a $^{19}$F pulse NMR spectrometer. The temperature was varied according to the following cycle: cooling from 393 to 203 K followed by heating to 393 K. Measurements were obtained every 10 K, keeping the temperature constant. The $T_1$ minimum point could not be clearly recognised after crystallisation.

during cooling (black symbols in Fig. 7) and 303 K during heating (red symbols in Fig. 7), which correspond to the crystallisation and melting temperatures, respectively. Note that the change in the $^{19}$F $T_1$ values after crystallisation was only slight in the range from 280 to 240 K. Hence, clearly identifying a minimum value for $T_1$ was not possible. This behaviour suggests the presence of plural $T_1$ minima distributed over a wide temperature range due to the flexibility around the two N–S and S–$CF_3$ axes of the $[NTf_2]^-$ ion in the crystalline state. All of the $[NTf_2]^-$ ions in [$C_1$mim][$NTf_2$] have been reported to adopt the cisoid conformation in the crystalline state.[66] The flexibility of the $[NTf_2]^-$ ion has been suggested by the small energy differences associated with large geometrical variations.[67,68] Therefore, it is possible that even in the crystalline state of [$C_1$mim][$NTf_2$], the cisoid conformation is an average conformation, and the $[NTf_2]^-$ ions move with large amplitudes.

The $^{1}$H $T_1$ and $T_2$ values for [$C_1$mim][$NTf_2$] as a function of temperature are plotted in Fig. 8. Discontinuous changes in these values occurred near 283 and 303 K, which are the same temperatures observed for the $^{19}$F $T_1$ and $T_2$ curves and correspond to the crystallisation and melting processes, respectively. After crystallisation, the $T_1$ values linearly (on a logarithmic scale in Fig. 8) decreased to a minimum at 213 K as the temperature decreased. Unlike for the $^{19}$F $T_1$ curve, however, only one minimum point was recognised, which suggested that the two methyl-groups in the cation likely had the same dynamics. In addition, the temperature of the $^{1}$H $T_1$ minimum point for [$C_1$mim][$NTf_2$] was lower than that for [$C_1$mim][FSA], and the activation energy for [$C_1$mim][$NTf_2$] (estimated from the linear part of the $T_1$ curve from 233 to 293 K) of approximately 8.7 kJ $mol^{-1}$ was also less than that for [$C_1$mim][FSA]. This smaller value indicated that in the crystalline state, the methyl groups in the cation of [$C_1$mim][$NTf_2$] could move more easily than those in the cation of [$C_1$mim][FSA].

 

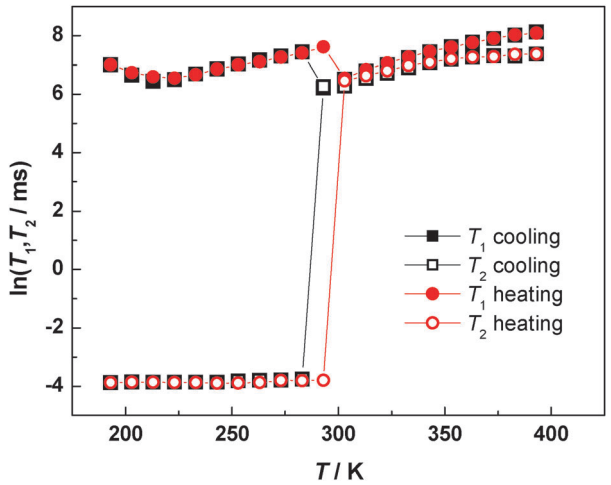


Fig. 8 $^{1}H$ $T_1$ and $T_2$ values for $[C_1mim][NTf_2]$ as a function of temperature obtained using a $^{1}H$ pulse NMR spectrometer. The temperature variation was performed in the same manner as described in Fig. 7. The minimum point in the $T_1$ trace for the crystalline state appeared at 213 K.

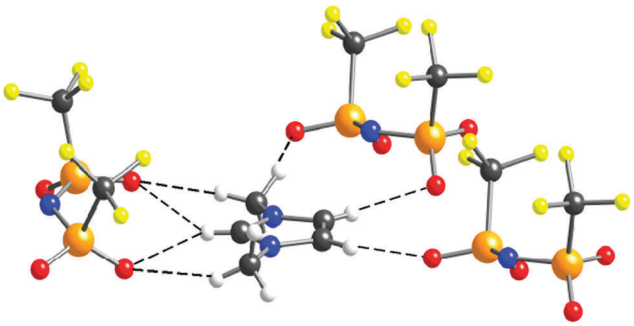

Fig. 9 Hydrogen bonding in a $[C_1mim][NTf_2]$ crystal (drawn according to ref. 66). Grey: carbon, blue: nitrogen, yellow: fluorine, orange: sulfur, red: oxygen and white: hydrogen.

Similar to the behaviour observed for $[C_1mim][FSA]$, the $^{1}H$ $T_1$ values for $[C_1mim][NTf_2]$ during cooling (black closed squares in Fig. 8) jumped to higher values during the phase change from the liquid to the crystalline state at 283 K, while the $^{19}F$ $T_1$ values (black closed squares in Fig. 7) jumped to lower values. The explanation for these trends is also similar to that given for $[C_1mim][FSA]$. The imidazolium moiety and the methyl groups are distinctly separate from the viewpoint of movement. The imidazolium ring position is frozen at the time of crystallisation, while the methyl groups can still rotate. Therefore, the rotation of the methyl groups in the crystalline state is the only contribution that the cation in $[C_1mim][NTf_2]$ makes to the $^{1}H$ $T_1$ (see eqn (5)). In contrast, in the $[NTf_2]^-$ ion, the entire ion moves, because the $CF_3SO_2$ groups rotate around the N–S axes and the $CF_3$ groups rotate around the S–C axes. Therefore, separating the movement of the anion into the individualised movements of different groups is impossible.

Furthermore, note that the jump width for the $^{19}F$ $T_1$ values of $[C_1mim][NTf_2]$ (Fig. 7) was remarkably wider than that for the $^{19}F$ $T_1$ values of $[C_1mim][FSA]$ (Fig. 3). This result indicated that the motions of the F atoms were likely different in the liquid and crystalline states due to an increase in bulkiness resulting from the exchange of F atoms for $CF_3$ groups.

Holbrey *et al.* reported the crystal structure of $[C_1mim][NTf_2]$.[66] Because structural information provides a more detailed understanding of the dynamics of the salt, the features of the structure were considered with respect to the results obtained in the present study. The arrangement of the $[NTf_2]^-$ ions around a $[C_1mim]^+$ ion, shown in Fig. 9, is based on the crystal data provided by Holbrey *et al.*,[66] with a focus on the structural interactions between the cation and the anion due to hydrogen bonding. In the crystalline state, the $[NTf_2]^-$ ion adopts a slightly distorted cisoid conformation. Similar to the structure of crystalline $[C_1mim][FSA]$, the structure of the $[C_1mim][NTf_2]$ crystal is characterised by three types of hydrogen bonds. The strongest hydrogen bond in the crystal is formed with two O atoms from the anion and three H atoms in the cation to generate a characteristic W-shaped tridentate hydrogen bonding arrangement, although it is slightly distorted (see Fig. 9). The second strongest hydrogen bond is formed with two O atoms from different anions and two H atoms bonded directly to an imidazolium ring. Both of these types of hydrogen bonds are formed in the imidazolium plane. As shown in Fig. 9, the third, weaker hydrogen bond is formed between two O atoms in different anions with two H atoms in the methyl groups in a single cation. In addition, as is the case for crystalline $[C_1mim][FSA]$, no F atoms participate in the hydrogen bonding in crystalline $[C_1mim][NTf_2]$. There are, however, two differences in the crystal structures of $[C_1mim][FSA]$ (Fig. 5(a) and (b)) and $[C_1mim][NTf_2]$ (Fig. 9): (i) in the $[C_1mim][NTf_2]$ crystal, other than in the W-shaped hydrogen bond, the $[C_1mim]^+$ ion forms hydrogen bonds with multiple anions, while in the $[C_1mim][FSA]$ crystal, the $[C_1mim]^+$ ion forms the 1 : 1 pair with the anion for each hydrogen bonding that is characterized by polydentate hydrogen bonding and (ii) the F atoms in the $[C_1mim][NTf_2]$ crystal can move relatively easily *via* rotation of the $CF_3$ groups because there is no restriction due to hydrogen bonding, while movement of the F atoms in $[C_1mim][FSA]$ is restricted due to the strong hydrogen bonding of the $SO_2$ groups, which are directly bonded to the F atoms. According to the packing structure, the $CF_3$ groups gather and form a sheet structure in the $[C_1mim][NTf_2]$ crystal,[66] and thus each $CF_3$ group exists in the weaker interaction field formed by other $CF_3$ groups. Hence, the F atoms in $[C_1mim][NTf_2]$ are thought to be able to move more freely.

Finally, both the $^{19}F$ $T_1$ and $^{1}H$ $T_1$ values for $[C_1mim][NTf_2]$ and $[C_1mim][FSA]$ gradually increased as the temperature decreased below 210 K due to a decrease in flexibility. However, the values for the $[C_1mim][NTf_2]$ crystal were much smaller than those for the $[C_1mim][FSA]$ crystal, which suggests that the former is much softer than the latter at the same temperature. This difference is thought to be due to the differences in the hydrogen bonding in the two RTILs as mentioned above in (i) and (ii).

## 4. Conclusions

Calorimetric data and the temperature dependence of the NMR relaxation times ($T_1$ and $T_2$) for the RTILs $[C_1mim][FSA]$ and

$[C_1mim][NTf_2]$ were evaluated. The $^{19}F$ relaxation times were suitable probes for studying the anion ($[FSA]^-$ and $[NTf_2]^-$) dynamics of the samples, while the behaviour of the $^1H$ relaxation times independently revealed the dynamics of the cation ($[C_1mim]^+$) in each RTIL. These data were then used to discuss the relationships between these behaviours. For both the samples, although the thermal histories observed according to the calorimetric and NMR analyses were different, the phase change temperatures determined in the calorimetric experiments agreed well with the temperatures at which the $T_1$ and $T_2$ values exhibited discontinuities. The results also indicated that each samples had a minimal thermal history.

With regard to $[C_1mim][FSA]$, crystallisation in the liquid state occurs due to a conformational change in the anions; namely, the portion of anions that exist in the transoid conformation in the liquid state changes to the cisoid conformation. At the same time, the systematic arrangement of the imidazolium cations occurs, because they are bound tightly to the cisoid anions. The melting process involves the opposite transformations. In addition, the methyl groups in the cation move even in the crystalline state, at least down to 210 K, with an estimated activation energy of 12.9 kJ $mol^{-1}$. Furthermore, the $T_1$ values for $^{19}F$ in the crystalline state are not very different from those for $^{19}F$ in the liquid state, suggesting that, with respect to the librational motion around the cisoid arrangement in the crystalline state, the $SO_2F$ groups move to the same extent as they do in the liquid state. Finally, on the whole, the cation and the anion exhibit cooperative motion, likely due to strong hydrogen bonding interactions.

With regard to $[C_1mim][NTf_2]$, crystallisation and melting are also caused by changes between the transoid and cisoid forms. However, there are two types of rotational freedom in the $[NTf_2]^-$ ion, namely rotation around the N–S axes and $CF_3$ rotation. In the crystalline state, the overlap of these two types of rotational dynamics was observed in the $T_1$ behaviours. In addition, as for crystalline $[C_1mim][FSA]$, the methyl groups in the cation of $[C_1mim][NTf_2]$ were found to move in the crystalline state, even at 210 K. However, the activation energy for $[C_1mim][NTf_2]$ was significantly less than that for $[C_1mim][FSA]$ at 8.7 kJ $mol^{-1}$. By evaluating both the $^{19}F$ and $^1H$ $T_1$ values, the former crystal was found to be much softer than the latter. These differences are likely due to differences in the hydrogen bonding interactions in the two RTILs and their free volumes, which are due to the different efficiencies of cation and anion packing. Specifically, for $[C_1mim][FSA]$, the volumes of the cation and the anion are nearly the same and thus very efficient and close packing is achieved in the crystalline state.[54]

Furthermore, note that sulfonylamide anions have conformational variations and flexibilities. The resultant and characteristic softness results in unique and effective functionality for these ionic groups as constituent anions in ionic liquids. The present study is one of a series of fundamental studies designed to reveal the dynamics of ionic liquids, including those with the simplest $[FSA]^-$ and second simplest $[NTf_2]^-$ ions and their related phase behaviours.

## Acknowledgements

This work was partially supported by MEXT KAKENHI (Grant number: 17073002) and JSPS KAKENHI (Grant number: 24655003). The NMR experiments for $^1H$ and $^{19}F$ were performed in Center for Analytical Instrumentation of Chiba University and in JEOL Ltd, respectively. The authors express sincere thanks to Mr Masahisa Sawada and Mr Takeyoshi Ikeda of JEOL Ltd for improvement of the MU-25 NMR apparatus for the present study.

## References

1 H. Hamaguchi and R. Ozawa, *Adv. Chem. Phys.*, 2005, **131**, 85–104.
2 Physical Chemistry of Ionic Liquids, Special issue of *J. Phys. Chem. B*, ed. J. F. Wishart and E. W. Castner, Jr, 2007, **111**(18).
3 Ionic Liquids, Special issue of *Acc. Chem. Res.*, ed. R. D. Rogers and G. A. Voth, 2007, **40**(11).
4 J. F. Wishart and E. W. Castner, Jr, *J. Chem. Phys.*, 2010, **132**, 120901.
5 *Science of Ionic Liquids*, ed. K. Nishikawa, Y. Ouchi, T. Itoh, H. Ohno and M. Watanabe, Maruzen, Tokyo, Japan, 2012, in Japanese.
6 T. Welton, *Chem. Rev.*, 1999, **99**, 2071–2083.
7 M. J. Earle and K. R. Seddon, *Pure Appl. Chem.*, 2000, **72**, 1391–1398.
8 J. S. Wilkes, *Green Chem.*, 2002, **4**, 73–80.
9 Ionic Liquids – Industrial Applications for Green Chemistry, ed. R. D. Rogers and K. R. Seddon, ACS Symp. Ser. 818, *Am. Chem. Soc.*, Washington DC, 2002.
10 *Ionic Liquids in Syntheses*, ed. P. Wasserscheid and T. Welton, VCH-Wiley, Weinheim, Germany, 2003.
11 J. Dupont, R. F. de Souza and P. A. Z. Suarez, *Chem. Rev.*, 2002, **102**, 3667–3692.
12 T. Welton, *Coord. Chem. Rev.*, 2004, **248**, 2459–2477.
13 *Electrochemical Aspects of Ionic Liquids*, ed. H. Ohno, Wiley-Interscience, Hoboken, 2005.
14 N. V. Plechkova and K. R. Seddon, *Chem. Soc. Rev.*, 2008, **37**, 123–150.
15 T. L. Greaves and C. J. Drummond, *Chem. Rev.*, 2008, **108**, 206–237.
16 J. D. Holbray and K. R. Seddon, *J. Chem. Soc., Dalton Trans.*, 1999, 2133–2139.
17 H. L. Ngo, K. LeCompte, L. Hargens and A. B. McEwen, *Thermochim. Acta*, 2000, **357**, 97–102.
18 J. G. Huddleston, A. E. Visser, W. M. Reichert, H. D. Willauer, G. A. Broker and R. D. Rogers, *Green Chem.*, 2001, **3**, 156–164.
19 C. P. Fredlake, J. M. Crosthwaite, D. J. Hert, S. N. V. K. Aki and S. N. Brennecke, *J. Chem. Eng. Data*, 2004, **49**, 954–964.
20 Y. U. Paulechka, G. J. Kabo, A. V. Blokhin, A. S. Shaplov, E. I. Lozinskaya and Y. S. Vygodskii, *J. Chem. Thermodyn.*, 2007, **39**, 158–166.
21 K. N. Marsh, J. A. Boxall and R. Lichtenthaler, *Fluid Phase Equilib.*, 2004, **219**, 93–98.

22 K. Nishikawa, S. Wang, H. Katayanagi, S. Hayashi, H. Hamaguchi, Y. Koga and K. Tozaki, *J. Phys. Chem. B*, 2007, **111**, 4894–4900.
23 K. Nishikawa, S. Wang and K. Tozaki, *Chem. Phys. Lett.*, 2008, **458**, 88–91.
24 K. Nishikawa and K. Tozaki, *Chem. Phys. Lett.*, 2008, **463**, 369–372.
25 K. Nishikawa, S. Wang, T. Endo and K. Tozaki, *Bull. Chem. Soc. Jpn.*, 2009, **82**, 806–812.
26 T. Endo, T. Kato, K. Tozaki and K. Nishikawa, *J. Phys. Chem. B*, 2010, **114**, 407–411.
27 T. Endo, T. Kato and K. Nishikawa, *J. Phys. Chem. B*, 2010, **114**, 9201–9208.
28 N. Shamin and G. B. McKenna, *J. Phys. Chem. B*, 2010, **114**, 15942–15952.
29 M. Imanari, K. Fujii, T. Endo, H. Seki, K. Tozaki and K. Nishikawa, *J. Phys. Chem. B*, 2012, **116**, 3991–3997.
30 J. D. Holbrey, W. M. Reichert, M. Nieuwenhuyzen, S. Johnston, K. R. Seddon and R. D. Rogers, *Chem. Commun.*, 2003, 1636–1637.
31 S. Hayashi, R. Ozawa and H. Hamaguchi, *Chem. Lett.*, 2003, 498–499.
32 R. Ozawa, S. Hayashi, S. Saha, A. Kobayashi and H. Hamaguchi, *Chem. Lett.*, 2003, 948–949.
33 R. W. Berg, *Monatsh. Chem.*, 2007, **138**, 1045–1075, and references cited therein.
34 T. Endo, K. Tozaki, T. Masaki and K. Nishikawa, *Jpn. J. Appl. Phys.*, 2008, **47**, 1775–1779.
35 T. Endo and K. Nishikawa, *J. Phys. Chem. A*, 2008, **112**, 7543–7550.
36 Y. Dong, *Prog. Nucl. Magn. Reson. Spectrosc.*, 2002, **41**, 115–151.
37 D. Bankmann and R. Giernoth, *Prog. Nucl. Magn. Reson. Spectrosc.*, 2007, **51**, 63–90.
38 J. H. Ansony, D. T. Mertens, A. Dölle, P. Wasserscheid and W. G. Carper, *ChemPhysChem*, 2003, **4**, 588–594.
39 J. H. Ansony, D. Mertens, T. Breitenstein, A. Dölle, P. Wasserscheid and W. R. Carper, *Pure Appl. Chem.*, 2004, **76**, 255–261.
40 W. R. Carper, P. G. Wahlbech and A. Dölle, *J. Phys. Chem. A*, 2004, **108**, 6096–6099.
41 S. H. Chung, R. Lopato, S. G. Greenbaum, H. Shirota, E. W. Castner Jr and J. F. Wishart, *J. Phys. Chem. B*, 2007, **111**, 4855–4893.
42 K. Hayamizu, S. Tuzuki and S. Seki, *J. Phys. Chem. A*, 2008, **112**, 12027–12036.
43 M. Imanari, M. Nakakoshi, H. Hiroko and K. Nishikawa, *Chem. Phys. Lett.*, 2008, **459**, 89–93.
44 M. Imanari, K. Uchida, K. Miyano, H. Seki and K. Nishikawa, *Phys. Chem. Chem. Phys.*, 2010, **12**, 2959–2967.
45 T. Endo, M. Imanari, H. Seki and K. Nishikawa, *J. Phys. Chem. A*, 2011, **115**, 2999–3005.
46 T. Endo, S. Widgeon, P. Yu, S. Sen and K. Nishikawa, *Phys. Rev. B: Condens. Matter Mater. Phys.*, 2012, **85**, 054307.
47 T. Endo, H. Murata, M. Imanari, N. Mizushima, H. Seki and K. Nishikawa, *J. Phys. Chem. B*, 2012, **116**, 3780–3788.
48 T. Endo, H. Murata, M. Imanari, N. Mizushima, H. Seki, S. Sen and K. Nishikawa, *J. Phys. Chem. B*, 2013, **117**, 326–332.
49 J. Foropoulos and D. D. DesMarteau, *Inorg. Chem.*, 1984, **23**, 3720–3723.
50 P. Johansson, J. Tegenfeldt and J. Lindgren, *J. Phys. Chem. A*, 2000, **104**, 954–961.
51 J. D. Holbrey, W. M. Reichert and R. D. Rogers, *Dalton Trans.*, 2004, 2267–2271.
52 K. Fujii, A. Seki, S. Fukuda, R. Kanzaki, T. Takamuku, Y. Umebayashi and S. Ishiguro, *J. Phys. Chem. B*, 2007, **111**, 12829–12833.
53 P. Bonhôte, A. P. Dias, N. Papageorgiou, K. Kalyanasundaram and M. Grätzel, *Inorg. Chem.*, 1996, **35**, 1168–1178.
54 K. Fujii, T. Mukai and K. Nishikawa, *Chem. Lett.*, 2014, 405–407.
55 T. C. Farrar and E. D. Becker, *Pulse and Fourier Transform NMR, Introduction to Theory and Method*, Academic Press, New York, 1971.
56 J. L. Markley, W. J. Horsley and M. P. Klein, *J. Chem. Phys.*, 1971, **55**, 3604–3605.
57 H. Y. Carr and E. M. Purcell, *Phys. Rev.*, 1954, **94**, 630–642.
58 S. Meiboom and D. Gill, *Rev. Sci. Instrum.*, 1958, **29**, 688–691.
59 P. Mansfield, *Phys. Rev.*, 1965, **137**, 961–974.
60 J. G. Powels and J. H. Strenge, *Proc. Phys. Soc.*, 1963, **82**, 6–15.
61 N. Bloembergen, E. M. Purcell and R. V. Pound, *Phys. Rev.*, 1948, **73**, 679–712.
62 I. Solomon, *Phys. Rev.*, 1955, **99**, 559–565.
63 Y. Inamura, O. Yamamuro, S. Hayashi and H. Hamaguchi, *Phys. B*, 2006, **385–386**, 732–734.
64 L. Xue, C. W. Padgett, D. D. DesMarteau and W. T. Pennington, *Solid State Sci.*, 2002, **4**, 1535–1545.
65 J. N. C. Lopes, K. Shimizu, A. A. H. Padua, Y. Umebayashi, S. Fukuda, K. Fujii and S. Ishiguro, *J. Phys. Chem. B*, 2008, **112**, 9449–9455.
66 J. D. Holbrey, W. M. Reichert and R. D. Rogers, *Dalton Trans.*, 2004, 2267–2271.
67 P. Johansson, S. P. Geijji, J. Tegenfeldt and J. Lindgren, *Electrochim. Acta*, 1998, **43**, 1375–1379.
68 M. Herstedt, M. Smirnov, P. Johansson, M. Chami, J. Grondin, L. Servant and J. C. Lassegues, *J. Raman Spectrosc.*, 2005, **36**, 762–770.